

Optimized parallel transmit and receive radiofrequency coil for ultrahigh-field MRI of monkeys



Kyle M. Gilbert^{a,*}, Joseph S. Gati^a, Kevin Barker^{a,b}, Stefan Everling^{a,c}, Ravi S. Menon^{a,d}

^a Centre for Functional and Metabolic Mapping, The University of Western Ontario, London, ON, Canada

^b Neuronitek, London, ON, Canada

^c Department of Physiology and Pharmacology, The University of Western Ontario, London, ON, Canada

^d Department of Medical Biophysics, The University of Western Ontario, London, ON, Canada

ARTICLE INFO

Article history:

Received 21 April 2015

Accepted 19 October 2015

Available online 20 October 2015

Keywords:

Transmit coil

Receive coil

Monkey

Parallel transmit

Echo-planar imaging

ABSTRACT

Monkeys are a valuable model for investigating the structure and function of the brain. To attain the requisite resolution to resolve fine anatomical detail and map localized brain activation requires radiofrequency (RF) coils that produce high signal-to-noise ratios (SNRs) both spatially (image SNR) and temporally. Increasing the strength of the static magnetic field is an effective method to improve SNR, yet this comes with commensurate challenges in RF coil design. First, at ultrahigh field strengths, the magnetic field produced by a surface coil in a dielectric medium is asymmetric. In neuroimaging of rhesus macaques, this complex field pattern is compounded by the heterogeneous structure of the head. The confluence of these effects results in a non-uniform flip angle, but more markedly, a suboptimal circularly polarized mode with reduced transmit efficiency. Secondly, susceptibility-induced geometric distortions are exacerbated when performing echo-planar imaging (EPI), which is a standard technique in functional studies. This requires receive coils capable of parallel imaging with low noise amplification during image reconstruction. To address these challenges at 7 T, this study presents a parallel (8-channel) transmit coil developed for monkey imaging, along with a highly parallel (24-channel) receive coil. RF shimming with the parallel-transmit coil produced significant advantages—the transmit field was 38% more uniform than a traditional circularly polarized mode and 54% more power-efficient, demonstrating that parallel-transmit coils should be used for monkey imaging at ultrahigh field strengths. The receive coil had the ability to accelerate along an arbitrary axis with at least a three-fold reduction factor, thereby reducing geometric distortions in whole-brain EPI.

© 2015 Elsevier Inc. All rights reserved.

Introduction

Neuroimaging of monkeys is an important means for investigating neuronal anatomy and function, including connectivity between neural networks and the blood-oxygenation-level dependent (BOLD) response (Barazany and Assaf, 2012; Dubowitz et al., 1998; Ekstrom et al., 2008; Logothetis et al., 1999, 2001; Moeller et al., 2008; Vanduffel et al., 2001). To discriminate the BOLD response originating from disparate locations in the brain, high-resolution functional imaging, as well as high-resolution anatomical references, are required (Chen et al., 2012, 2013; Goense et al., 2012; Logothetis et al., 2002). To resolve such fine anatomical and functional detail places stringent demands on the performance characteristics of the radiofrequency (RF) coil. Most notably, the RF coil must be highly sensitive, equating to a high signal-to-noise ratio (SNR). The most effective method to improve sensitivity is to

situate the coil in close proximity to the head; however, in monkeys, this is made difficult by the presence of head-fixation posts, recording chambers (used for electrophysiological measurements), and external hardware affixed to the skull. The large lateral muscles on the monkey head further distance the coil from the brain. A common method to improve the SNR of the MRI experiment is to increase the strength of the static magnetic field. Although it is an effective solution, an increase in field strength is accompanied by several challenges, most notably a non-uniform, and potentially inefficient, transmit field and the presence of susceptibility induced geometric distortions.

At ultrahigh field strengths, the magnetic field pattern of a surface coil becomes increasingly asymmetric in a dielectric medium (Wiesinger et al., 2004). This complex wave behavior, coupled with the non-uniform shape of the monkey head, causes the most efficient mode of a cylindrical transmit coil to deviate from an equally distributed 2π phase accrual about its circumference. This is further complicated when the wavelength of the transmit field approaches the width of the head ($\lambda/2 \sim 7\text{--}8$ cm *in vivo* at 7 T), causing a central-brightening effect due to the destructive interference of the transmit field in the periphery of the head. The combination of these effects can reduce the

* Corresponding author at: Centre for Functional and Metabolic Mapping, The University of Western Ontario, 1151 Richmond St. N, London, Ontario N6A 5B7, Canada. Fax: +1 519 931 5260.

E-mail address: kgilbert@robarts.ca (K.M. Gilbert).

transmit-field efficiency and uniformity. A variance of flip angle across the head can reduce the contrast between tissues, while a lower efficiency can restrict the amplitude and duty cycle of RF pulses due to constraints imposed by the power amplifier or specific absorption rate (SAR). To mitigate these problems, multi-channel transmit coils have been developed (Adriany et al., 2010a; Gilbert et al., 2010). The magnitude and phase of each transmit channel can be chosen to improve the efficiency and/or uniformity of the transmit field, a process known as RF shimming (Mao et al., 2006; Van de Moortele et al., 2005).

A second problem at ultrahigh field strengths occurs when magnetic-susceptibility gradients at tissue–air interfaces cause large inhomogeneities in the local magnetic field. Magnetic-susceptibility gradients are particularly prevalent in the monkey brain due to the presence of large nasal cavities and the potential for external hardware to be affixed to the skull. This, in turn, causes geometric distortions in echo-planar imaging (EPI)—a technique that is ubiquitous in the acquisition of fMRI datasets. Geometric distortions can be mitigated by shortening the echo train with parallel imaging (Pruessmann et al., 1999; Sodickson and Manning, 1997) and with partial-Fourier encoding. Therefore, effective functional imaging at ultrahigh field strengths requires an array of receive elements that produce low noise amplification during reconstruction of under-sampled data. To minimize noise

amplification, receive elements must be highly decoupled and have independent field profiles.

Numerous designs for RF coils have been devised for monkey imaging. At 3 T, quadrature transceive coils (Roopnariane et al., 2012), and volume transmit coils combined with receive arrays with up to 22 elements (Helms et al., 2013; Janssens et al., 2012, 2013; Khachaturian, 2010; You et al., 2007), have been used for whole-brain imaging. At ultrahigh field (7 T), whole-brain imaging has been accomplished with volume transceive coils (Gonen et al., 2008; Pfeuffer et al., 2004) and with volume transmit coils combined with receive arrays consisting of up to eight elements (Kolster et al., 2007; Mareyam et al., 2011; Papoti et al., 2013). Small-diameter surface coils have also been implemented as a means to improve SNR over a localized region for high-resolution functional imaging (Goense et al., 2010; Logothetis et al., 2002; Pfeuffer et al., 2004, 2007). Although multi-transmit coils have been more commonly implemented in combination with receive arrays for human studies, for example of the spine (Zhao et al., 2014) and head (Adriany et al., 2012), to date, only a limited number of multi-transmit studies on monkeys have been performed (Adriany et al., 2010b; Gilbert et al., 2013; Zitella et al., 2015), while most coil systems rely on quadrature or single-channel transmit coils to provide excitation.

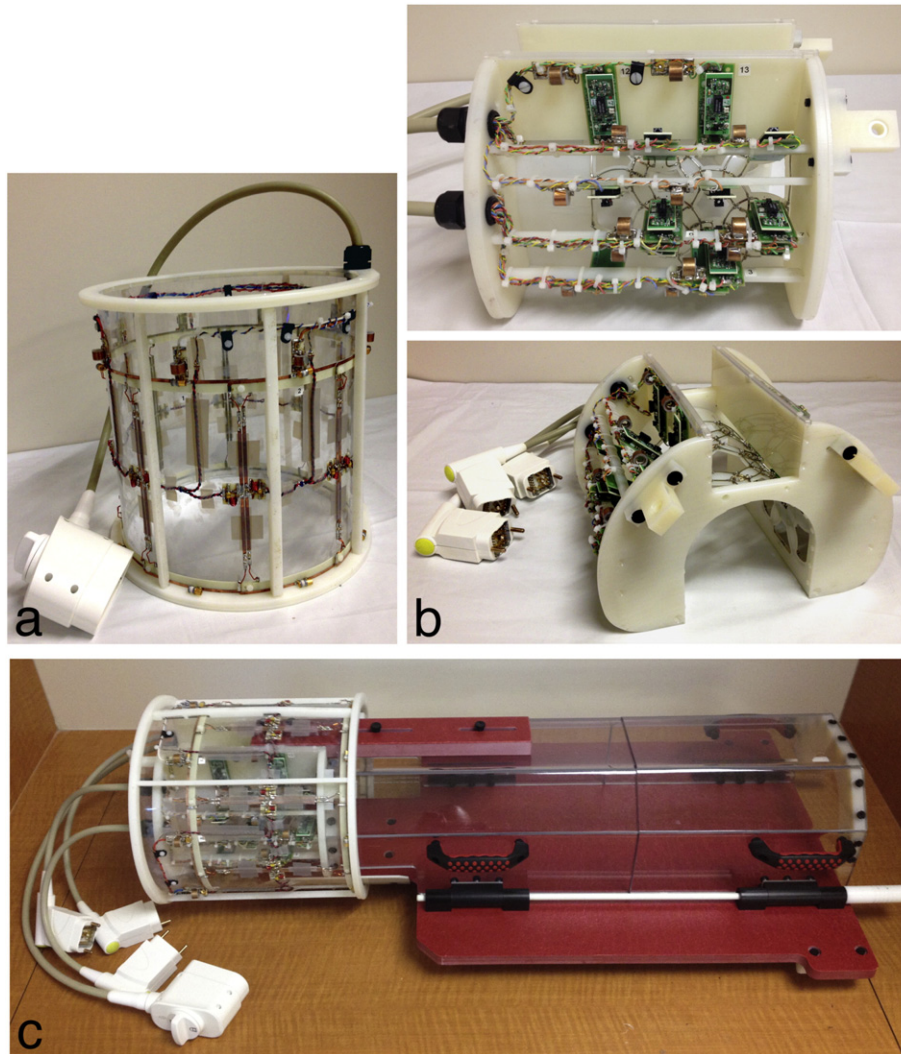


Fig. 1. Photographs of (a) the transmit coil, (b) two views of the receive coil, and (c) both coils together with the restraint system. Physiological monitoring equipment was attached to the monkey while no coil was present. The receive coil was then attached to the restraint system, after which the head-fixation post of the monkey was secured to the immobilization bar. The receive coil and restraint system were then slid into the transmit coil while on the scanner bed.

In this study, an RF coil system was developed to address the challenges inherent to whole-brain imaging of monkeys at 7 T. We investigate whether parallel-transmit coils are beneficial for ultrahigh-field monkey imaging and investigate the effectiveness of a highly parallel receive array. The RF coil included an 8-channel transmit array and a 24-channel receive array. The parallel-transmit coil was used to address non-uniformities in the transmit field and to improve transmit efficiency through RF shimming. The receive coil was designed for whole-brain imaging and allowed for parallel acceleration along an arbitrary axis to reduce geometric distortion during functional imaging. High-resolution anatomical images and echo-planar time-series data were acquired to demonstrate image quality.

Materials and methods

Transmit coil

The transmit coil (Fig. 1a) consisted of eight rectangular loops (width: 11.8 cm, length: 22.2 cm) circumscribing a 28.6-cm-diameter former. The former was constructed of clear polycarbonate to allow visual assessment of the monkey during setup. Adjacent elements of the transmit coil were overlapped to decrease through-space inductive coupling. Wire jumpers on the element legs were bent to adjust the overlap between adjacent elements and optimize decoupling; the optimal overlap was approximately 4–5 mm. Next-nearest-neighbor elements were circumferentially 90° apart, and therefore were intrinsically well decoupled—no additional decoupling circuitry was required.

Elements were milled out of 36- μm -thick copper adhered to 0.79-mm-thick garolite and had trace widths of 3 mm. The corners of elements were filleted to reduce radiation losses and dielectric coupling to the sample. Six surface-mount capacitors (100 series, American Technical Ceramics, NY, USA) were incorporated into each element. Variable capacitors (1.5–19 pF, model 55H01, Johanson

Manufacturing, NJ, USA) were placed at the drive point and opposite thereof to allow the element to be tuned to 297 MHz and matched to 50 Ω . Coil elements were matched to 50 Ω , using the ratio of the parallel-to-series capacitance, when loaded with a 50-mM NaCl phantom representing a typical head size of a rhesus macaque. When the sample size was varied, there was a negligible shift in resonant frequency and less than a 2- Ω change in impedance; therefore, coil elements were tuned and matched once on the bench and not prior to each experiment.

A choke balun was placed at the input of each transmit element to reduce common-mode currents and create a balanced drive to the coil. Choke baluns consisted of a two-loop inductor wound with semi-rigid coaxial cable (UT-85C-FORM, Micro-coax, PA, USA). The inductor was shielded by copper tape mounted on a 1.3-cm-diameter nylon tube. A 13-pF surface-mount capacitor bridged the inductor to create a parallel resonance on the coaxial shield at 297 MHz.

Active detuning was incorporated into each coil element using two parallel-resonant circuits located symmetrically in the central axial plane of the coil element. Twisted pairs of 24-gauge insulated wire were used for DC biasing and were routed along the virtual ground of the coil. Multiple RF chokes (1- μH inductors with a self-resonance frequency of approximately 300 MHz; series AISC-1008, Abracon Corporation) were incorporated into each DC line. The pin diode (HUM2020, Microsemi, CA, USA) of the detuning circuit was forward-biased (100 mA) during signal reception, resulting in a high-impedance circuit. A reverse voltage (–30 V) was applied during transmission. A circuit schematic of a transmit element is provided in Fig. 2a.

Receive coil

The receive coil consisted of wire loops arranged on an inverted U-shaped nylon former (nominal diameter: 12.7 cm, length: 15.6 cm, height: 11.3 cm). Loops were constructed of 16-gauge tinned copper

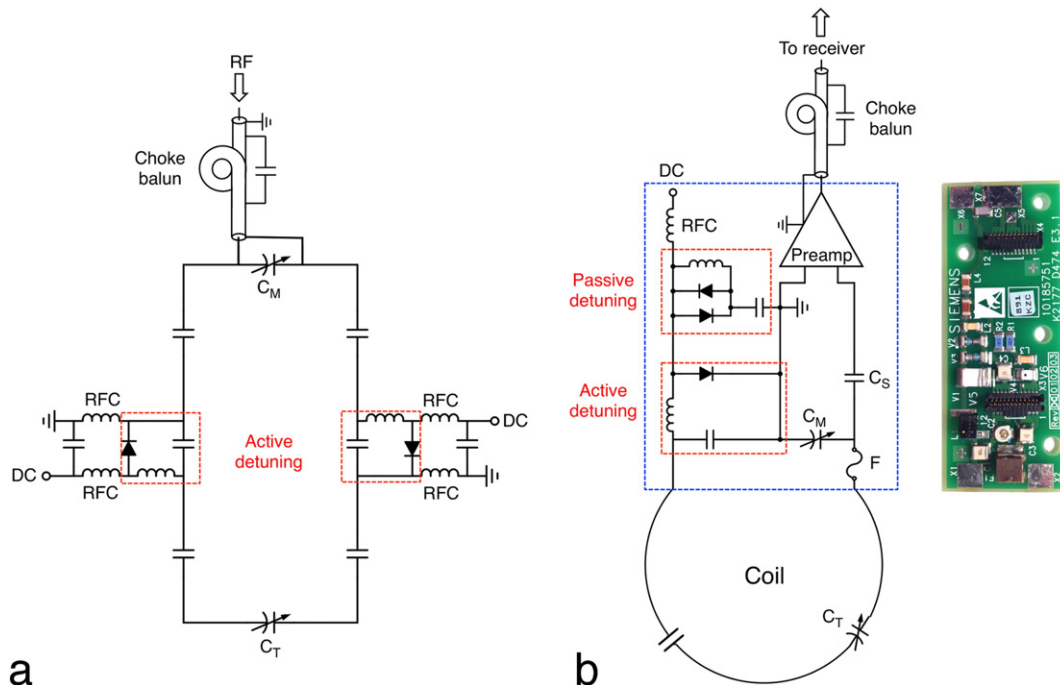


Fig. 2. (a) A circuit schematic of a transmit element. The coil element is tuned to 297 MHz and matched to 50 Ω by adjusting the ratio of the matching capacitor, C_M , and tuning capacitor, C_T . Two active detuning circuits are integrated into each coil element to reduce coupling to the receive coil during reception. (b) A simplified schematic (some components have been omitted for clarity) of a receive element showing the passive and active detuning networks. All components within the blue dashed line belong to the commercial matching board (right-hand photograph with the preamplifier removed [Siemens Healthcare, Erlangen, Germany]). The serial capacitor, C_S , is adjusted to fine-tune preamplifier decoupling, while C_T and C_M are used to tune and match the coil to minimize the noise figure of the preamplifier. A fuse, F , is integrated into the circuit for additional protection to the subject.

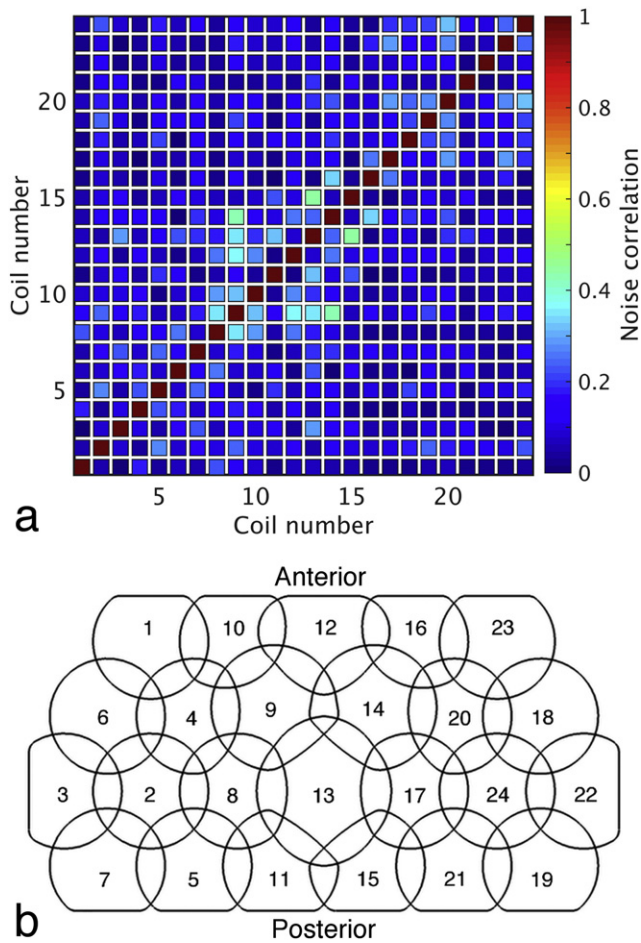


Fig. 3. (a) Noise correlation matrix for the 24-channel receive coil when acquired with a 50-kHz bandwidth. Coil numbers refer to the layout provided in (b). The highest noise correlation occurred at the superior apex of the coil, where elements of varying size were required to accommodate a head-fixation post and cables for recording devices. (b) A planar schematic depicting the coil layout. The coil layout wrapped around an inverted U-shaped former (see Fig. 1b), with the most superior elements located approximately 1 cm from the head and lateral elements located approximately 3 cm from the head.

wires. Intersections between loops were milled from copper-clad garolite and wire jumpers were implemented at the intersections between coils. This allowed the overlap between coil elements to be readily modified to decrease the mutual inductance between adjacent elements. Loop diameters ranged from 5–7 cm with the larger loops residing at the superior aspect of the head to accommodate a head-fixation post and cables for recording devices—portions of the former surface that were not directly attached to a coil element were removed. The layout of the receive coil was designed following the guidelines described by Roemer et al. (1990) and was comprised of four rows of coil elements. The four rows consisted of a different number of elements (6–7–6–5, from posterior to anterior, respectively) with the shape of peripheral elements adapted to fit the surface area of the former. Each loop consisted of one 5.1-pF or 6.2-pF surface-mount capacitor (100 series, American Technical Ceramics, NY, USA) and one variable capacitor (3–10 pF, Sprague-Goodman Electronics, Inc., NY, USA) for tuning.

Low-input-impedance preamplifiers (Siemens Healthcare, Erlangen, Germany) were mounted directly on each coil element and therefore had a symmetric input. The orientation of preamplifiers, in relation to the main magnetic field, was chosen to minimize the Hall effect in accordance with the manufacturer's specifications. Preamplifiers had a maximum noise figure of 0.6 dB and a gain of 26 dB. Elements were matched to within $\pm 10 \Omega$ of 75Ω (i.e., the optimal noise match for the preamplifiers) by adjusting the ratio of the parallel-to-series

capacitance. The preamplifiers had a slowly varying degradation in noise figure with varying load, thereby accommodating a range of head sizes with a negligible reduction in SNR. No preamplifiers were located along a 7.6-cm-wide central gap (see Fig. 1b) to accommodate an immobilization bar that would screw onto the head-fixation post of the monkey.

A series variable capacitor was adjusted on the input circuit of the preamplifier to transform the low input impedance of the preamplifier to a high-impedance parallel-resonance across the matching capacitor of the coil. Active detuning was incorporated into the commercial matching board (Siemens Healthcare, Erlangen, Germany) of each preamplifier to detune the coil during RF transmission. A passive detuning network and a 315-mA fast-blow RF fuse were incorporated on the matching board as a contingency in case the active-detuning network

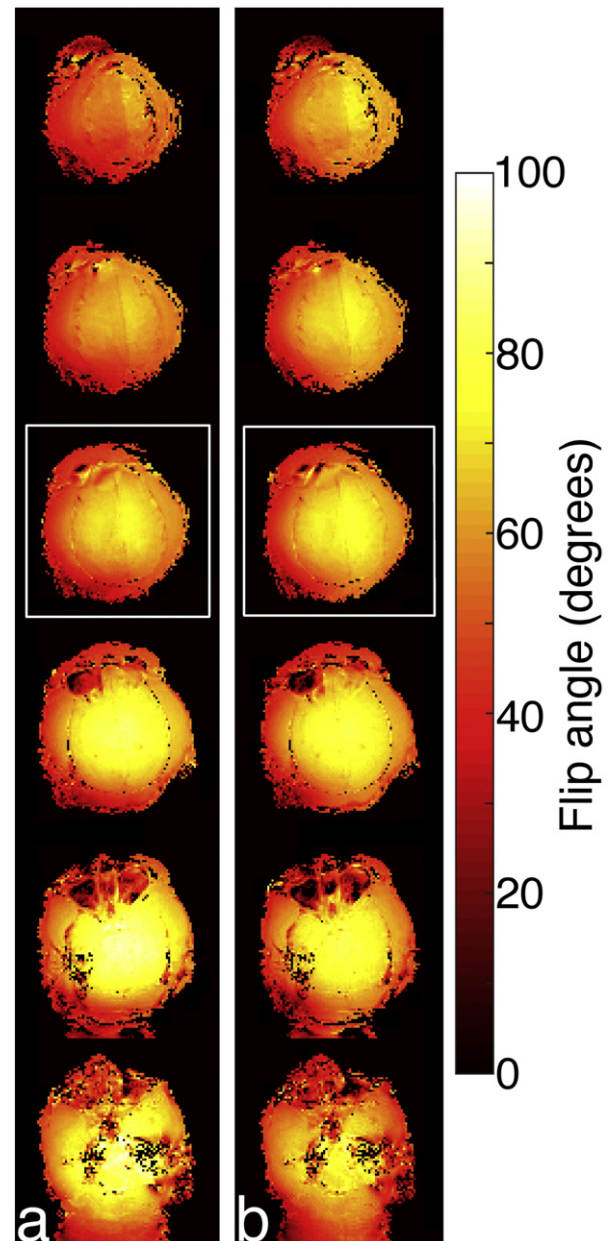


Fig. 4. Flip-angle maps covering the brain and lateral muscles, as acquired with (a) phases set to a circularly polarized mode ascertained in an oil phantom (with a reference voltage of 115 V per channel), and (b) the phase and magnitude of each transmit channel chosen to balance transmit efficiency and uniformity (with an average reference voltage of 88 V per channel). The mean flip angle over the brain was 71° for both shim solutions. The uniformity was calculated over the whole brain and over the slice denoted by white boxes.

failed. Choke baluns were placed on the output of each preamplifier to reduce common-mode currents induced by the transmit coil. A circuit schematic of a receive element is provided in Fig. 2b.

The monkey was enclosed in a custom-built restraint system comprised of a removable polycarbonate tube and a neck plate. After the monkey was placed in the restraint system, the receive coil could be mounted on the front panel of the restraint system. An immobilization bar would then be screwed onto the head-fixation post of the monkey. At this point, the monkey, restraint system, and receive coil would be slid into the transmit coil as a unit while on the scanner bed.

Bench measurements

S_{12} measurements of inductive coupling between adjacent elements, preamplifier decoupling, and active detuning were recorded when the coils were loaded with an 11.1-cm-diameter phantom filled with 50-mM sodium chloride (NaCl) and 20-mM copper sulphate (CuSO_4). Preamplifier decoupling and active detuning were measured with all coil elements in the completed array. The Q -ratio (unloaded-to-loaded $Q [Q_u/Q_l]$) was measured for an isolated element when loaded with a 50-mM NaCl sample with varying distance between the coil and sample.

Imaging

All MR data collection was performed on a human, head-only 7-T MRI scanner, controlled by a Step-2.1 console (Siemens Healthcare, Erlangen, Germany) with 32 receivers and independent control over the magnitude and phase of eight transmit channels. The system is equipped with an AC84 head gradient coil (maximum gradient strength: 80 mT/m, maximum slew rate: 400 mT/m/s, [Siemens Healthcare, Erlangen, Germany]) with a 36-cm-diameter clear bore. The Siemens head gradient coil included a slotted copper shield built into its inner diameter; the RF shield reduced coupling between RF coils and the gradient coil.

The transmit channels were powered by an eight-channel power amplifier with 1-kW peak power per channel. The transmit-amplifier output power (forward—reflected) was monitored during all scans. The losses in the RF pathway (including sources of power loss attributed to the transmit chain, radiation, RF shield, thermal noise, and the presence of the receive coil) were estimated. With consideration of these power losses and an estimate of the exposed tissue mass, the six-minute average power was limited to 20 W (at the amplifier) to allow

a maximum global SAR of 3 W/kg. The per-channel power was commensurately set to 2.5 W/channel (i.e., = 20 W/8 channels).

The front-end consisted of 32 independent receive chains, of which 24 were used for this study. All preamplifiers were located on the coil.

Animal Preparation

All imaging was performed on 6.5–8.5-kg rhesus macaque monkeys. Monkeys had dental acrylic implants affixed to the skull with multiple ceramic screws. A head-fixation post was embedded in the implant at the superior apex of the head. Monkeys were anesthetized with 1% isoflurane when acquiring EPI time series and with up to 2% isoflurane during anatomical scans. The monkey was placed headfirst in the sphinx position for imaging experiments. Animal handling and imaging was performed in accordance with an Animal Use Protocol approved by the University of Western Ontario.

RF shimming

Flip-angle maps were created for two different shim solutions. The first shim solution consisted of setting the phases of transmit channels to create a circularly polarized mode in an oil phantom, then implementing these phases *in vivo*—this was intended to mimic a volume coil driven with a fixed phase difference between ports of $2\pi/n$, where n is the number of channels, such as a birdcage coil. The circularly polarized mode was determined by measuring, and subsequently equalizing, the mean phase of each channel's transmit field over a $30 \times 30 \times 30$ mm region in the centre of the oil phantom. The second shim solution consisted of setting the phase and magnitude of each transmit channel using a least-squares optimization that balanced transmit efficiency and uniformity (Curtis et al., 2012). This shim solution was optimized over the whole brain to create a single shim setting suitable for three-dimensional acquisitions. The ROI (both size and orientation) over which RF shimming was applied was defined in all three dimensions using axial, coronal, and sagittal locator images, in the same manner as ROIs are typically defined in imaging sequences.

The actual flip-angle imaging (AFI) technique (Yarnykh, 2007), augmented with an RF and gradient spoiling scheme (Nehrke, 2009), was used to map the transmit field (matrix size: $96 \times 96 \times 20$, FOV: $12.8 \times 12.8 \times 10.2$ cm, TE/TR1/TR2: 3.0/20/100 ms, flip angle: 70° , BW: 1 kHz/pixel). Flip-angle maps were acquired with the reference voltage determined by the shimming algorithm. The uniformity of the transmit field was calculated from the AFI maps by normalizing the

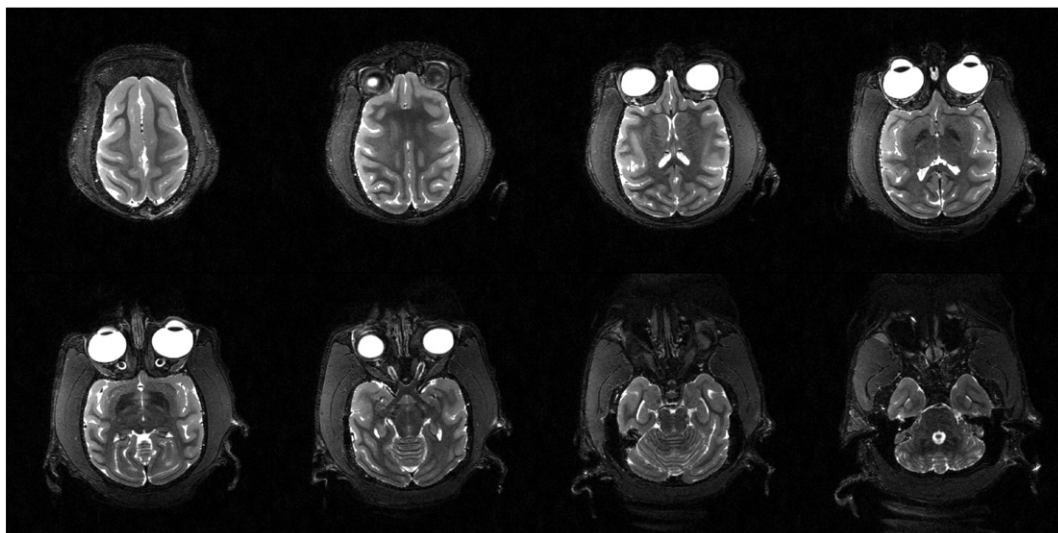


Fig. 5. Coronal slices of a TSE image acquired with 500- μm in-plane resolution and interpolated to 250- μm in plane for display purposes. RF shimming with the parallel transmit coil created a transmit field sufficiently uniform to create consistent contrast throughout the brain.

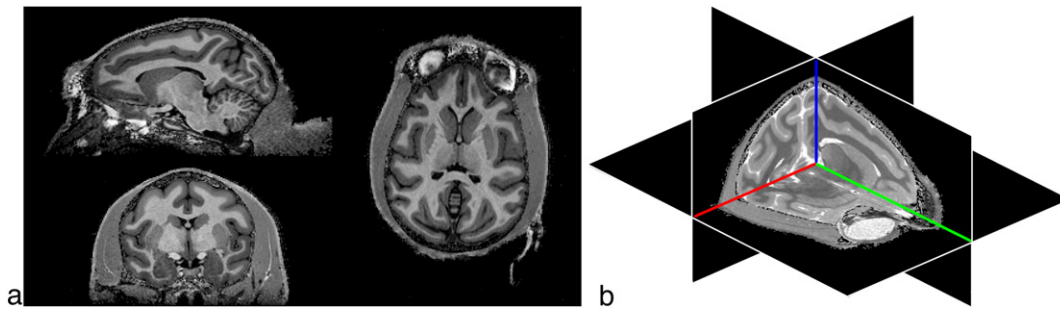


Fig. 6. (a) Three orthogonal slices of an MP2RAGE image acquired with 500- μm isotropic resolution, and (b) the commensurate 3D T_1 map. The adiabatic condition was realized throughout the brain, creating uniform contrast. Images were acquired with an acquisition time of 12 min 16 s.

standard deviation of the flip angle over the brain (excluding the lateral muscles) by the mean flip angle over the same region. The uniformity was also calculated over a single coronal slice.

Geometry-factor measurements

The noise amplification during parallel imaging was determined for the 24-channel receive coil. Coronal and sagittal fully sampled gradient-echo images were acquired (matrix: 192×192 , FOV: 12.0×12.0 cm, slice thickness: 5 mm, flip angle: 20° , TE/TR: 3.7/7.6 ms, BW: 250 Hz/pixel). Under-sampling of k-space was performed retrospectively with 2-, 3-, and 4-fold acceleration rates in one and two dimensions. Inverse geometry-factor (g -factor) maps were reconstructed using Matlab (The MathWorks, Natick, MA) by implementing the sensitivity encoding (SENSE) method (Pruessmann et al., 1999). Receiver noise correlation was calculated from the complex data of a bandwidth-matched, noise-only acquisition.

Imaging

A turbo-spin-echo (TSE) sequence, with 120° refocusing pulses, was acquired to evaluate transmit-field uniformity (matrix: 256×256 , FOV: 12.8×12.8 cm, number of slices: 40, slice thickness: 1 mm, slice gap: 0.1 mm, TE/TR: 90/7500 ms, BW: 219 Hz/pixel, echo train length: 8, echo spacing: 12.9 ms, acquisition time: 2 min 32 s). A reduction factor of two was implemented in the anterior-posterior direction with 31 reference lines. Whole-brain MP2RAGE images, with 500- μm isotropic resolution, were acquired to evaluate image quality (matrix: $256 \times 202 \times 128$, TE/TR: 3.2/6500 ms, T11/T12: 800/2700 ms, BW: 240 Hz/pixel, flip angle: $4^\circ/5^\circ$, acquisition time: 12 min 16 s). A reduction factor of two was utilized in the phase-encode direction (left-right) with 24 reference lines. All accelerated images were reconstructed

with generalized autocalibrating partially parallel acquisition (GRAPPA) (Griswold et al., 2002).

To investigate geometric distortions in whole-brain functional imaging, three single-shot EPI time series were acquired under different conditions: (1) with no acceleration or partial-Fourier encoding and the minimum possible TE value of 39 ms, (2) with a two-fold reduction factor in the anterior-posterior direction, 24 reference lines, three-quarter partial-Fourier encoding, and a matched TE value of 39 ms, and (3) with identical encoding as in (2), yet with the more realistic TE value for 7-T functional imaging of 20 ms. Time courses were acquired with all other parameters held constant (matrix: 96×96 , resolution: 1×1 mm, slice thickness: 1 mm, TR: 1000 ms, slices: 22, BW: 1680 Hz/pixel, flip angle: 40° , volumes: 300, acquisition time: 1 s/volume). In each dataset, two slices were acquired simultaneously using multiband EPI (Moeller et al., 2010). Temporal SNR (tSNR) maps were calculated by measuring the ratio of the mean signal of each pixel through the time course to the standard deviation of that pixel through the time course (Reeder, 2007).

Results

Active detuning of the transmit coil achieved a mean isolation ($S_{12, \text{detuned}} - S_{12, \text{tuned}}$) over all eight channels of -33 dB. The overlap between adjacent transmit elements was adjusted to achieve a minimum and mean S_{12} of -12 dB and -16 dB, respectively. The mean S_{12} between next-nearest neighbors was -20 dB, while the mean S_{12} over all element combinations was -21 dB. The receive coil had a mean S_{12} between adjacent elements of -13 dB and a mean preamplifier decoupling of -21 dB. This resulted in a mean and maximum noise correlation of 12% and 44%, respectively; Fig. 3 provides the full noise correlation matrix. Active detuning provided -40 dB of isolation during transmit. The Q -ratio of an isolated element varied from 2.0 ($=270/137$) to 3.8 ($=270/72$) depending on the degree of loading.

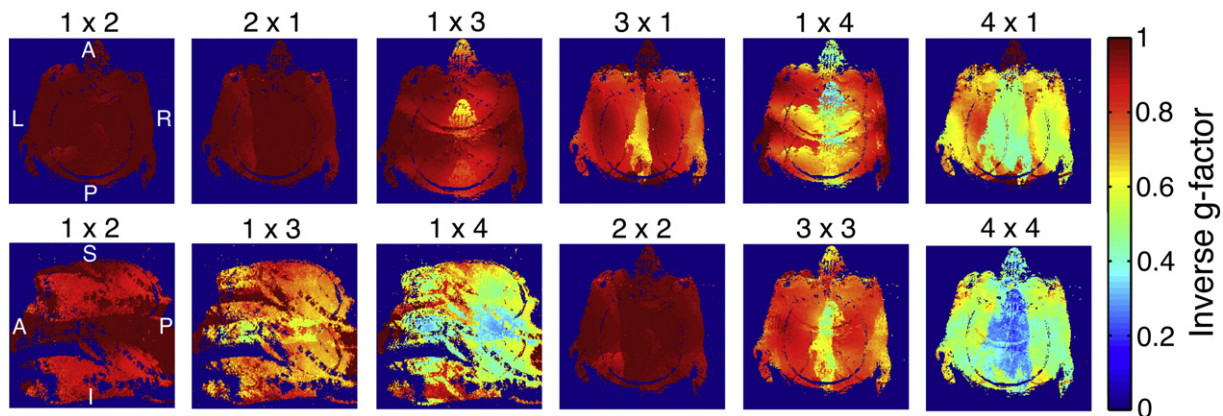


Fig. 7. Inverse g -factor maps produced by the receive coil. The reduction factor is provided above each map, and the maximum/mean g -factors are provided in Table 1. The receive coil consisted of 24 elements divided into four rows in the anterior-posterior direction.

Table 1

The mean and maximum g -factors for two-, three- and four-fold reduction factors, R , along each axis in the provided slice orientation.

	Mean	Maximum
$R = 2$		
Left–right (coronal)	1.03	1.30
Anterior–posterior (coronal)	1.02	1.10
Superior–inferior (sagittal)	1.21	1.62
$R = 3$		
Left–right (coronal)	1.20	2.29
Anterior–posterior (coronal)	1.10	1.80
Superior–inferior (sagittal)	1.37	2.54
$R = 4$		
Left–right (coronal)	1.68	4.06
Anterior–posterior (coronal)	1.40	4.75
Superior–inferior (sagittal)	1.82	4.22
$R = 2$ by 2		
Coronal	1.03	1.37
Sagittal	1.11	1.99
$R = 3$ by 3		
Coronal	1.31	2.65
Sagittal	1.69	4.18

Flip-angle maps are presented in Fig. 4. The transmit field produced by a circularly polarized mode (where phases were determined *a priori* on an oil phantom) had a reference voltage of 115 V per channel when calibrated *in vivo*. The circularly polarized mode was uniform to 15.6% over the whole brain and 9.7% over a single coronal slice (denoted by the white box in Fig. 4). When both the phase and magnitude were optimized, phases deviated from the circularly polarized mode by an average of 45° per channel, and the voltage weighting (magnitude) of channels ranged from 0.43 to 1.0 (mean: 0.76). The reference voltage was determined to be 116 V, equating to a mean reference voltage of 88 V per channel (*i.e.*, 76% of 116 V); therefore, the optimized shim solution required a 24% lower reference voltage and 54% less power than the circularly polarized mode. The transmit field was uniform to

8.9% over the whole brain and 7.7% over a single slice. This corresponds to a 38% and 13% improvement in uniformity over the whole brain and over a single slice, respectively, when compared to the circularly polarized mode.

Representative coronal slices of a TSE image are presented in Fig. 5. Images have not been corrected for receive sensitivity. Three planes of the 3D-MP2RAGE image, with 500- μm isotropic resolution, are shown in Fig. 6a. A byproduct of the MP2RAGE sequence is the creation of a T_1 map: the 3D T_1 map is shown in Fig. 7b.

For accelerated images, the spatial dependency of the SNR degradation is provided by the inverse g -factor, as shown in Fig. 7. The corresponding mean and maximum g -factors are provided in Table 1. The effect of echo-train length and TE value on geometric distortion and SNR in an EPI time series is presented in Fig. 8. Significant distortion and ghosting is present in the phase-encode direction of the fully encoded image. Shortening the echo train significantly reduced these artifacts, but decreased the mean temporal SNR over the slice by 21%; the decrease in SNR is mainly attributable to the lower fraction of encoded k -space, with an additional, yet minimal, contribution from the g -factor (see Table 1). Decreasing the echo time from 39 ms to 20 ms, with the equivalent Fourier encoding, improved the mean temporal SNR over the slice by 55%.

Discussion

Transmit-field efficiency and uniformity

Both shim solutions (*i.e.*, circularly polarized [representative of single-transmit volume coils] and when optimized for phase and magnitude [parallel transmit]) produced similar field patterns and exhibited the typical central brightening expected at ultrahigh field; however, non-uniformities in the transmit field and inefficiencies in the circularly polarized mode became more conspicuous when the transmit field was characterized over the whole brain. By RF shimming, the required

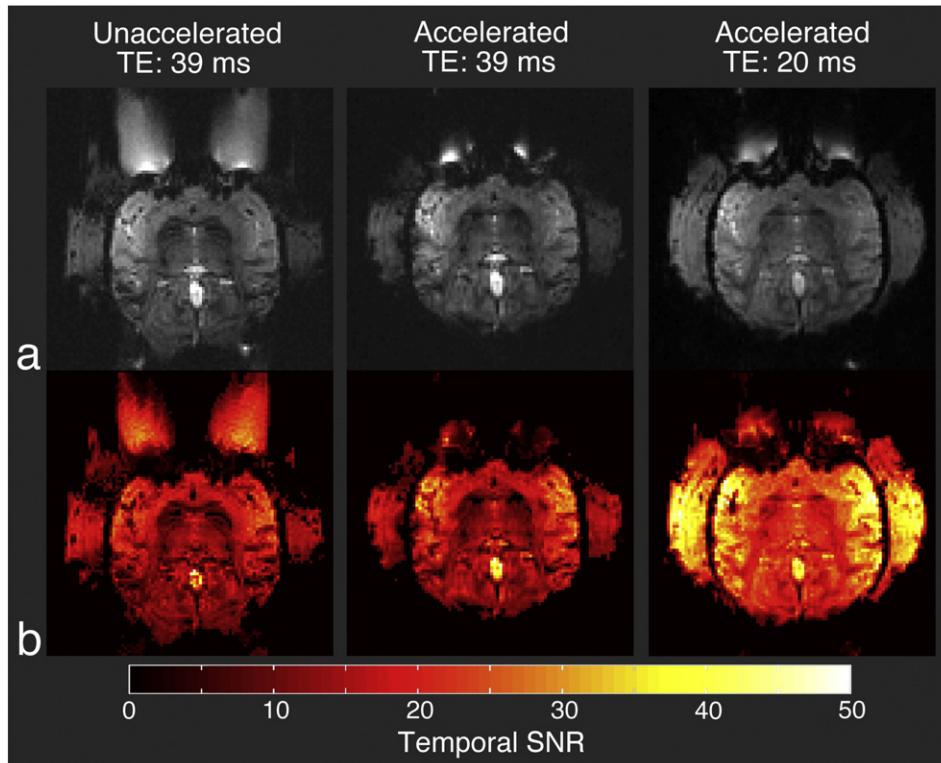


Fig. 8. (a) A single slice of three EPI time courses acquired with and without parallel acceleration and with different TE values. Geometric distortions are largely mitigated by shortening the echo train, while the corresponding temporal SNR, (b), is restored, and exceeded, by reducing the TE value.

transmit power was lowered by 54% and the uniformity was improved by 38% over the brain. This demonstrates that there is a discernible advantage to using parallel-transmit coils, in comparison to single-transmit volume coils, for even smaller sized objects at 7 T. The lower power requirements can be leveraged to acquire more slices per repetition time, to shorten RF pulses, or to invoke higher-power adiabatic pulses. Moreover, the RF shimming algorithm implemented in this study invokes a tradeoff between transmit uniformity and efficiency; the weighting of this tradeoff can be chosen to further improve one aspect over another to suit the needs of a particular imaging protocol.

Spin-echo derived sequences are the most demanding on transmit-field uniformity due to their train of high flip-angle refocusing pulses, yet the TSE image of Fig. 5 shows uniform contrast throughout the brain due to a low variation in flip angle across the imaging volume. The uniformity of the transmit field, combined with its high efficiency, allowed the adiabatic condition to be achieved throughout the brain in an MP2RAGE image, creating uniform contrast into the cerebellum and brain stem.

Image quality

The former of the receive coil was designed to fit close to the heads of different monkeys while avoiding the head-fixation post. This provided a practical means to perform routine scanning of a range of monkey sizes. Cutouts in the coil former allowed electrophysiological recording cables to be routed from various locations on the monkey head to outside of the coil.

MP2RAGE images (Fig. 6) demonstrate the whole-brain coverage possible with such a coil design, with high SNR inferior to the cerebellum and into the brain stem. Images show excellent coverage in the visual cortex, despite coils with sensitivity to this region being located at a greater distance than coils sensitive to the parietal or temporal lobes. The high SNR suggests the image can be acquired with an even higher resolution or acceleration rate without the necessity for multiple averages. The smaller diameter receive elements required for the 24-channel coil achieved Q -ratios that were body-noise dominated (up to 3.8) when located in close proximity to the sample, thereby allowing for a high sensitivity. Sensitivity could be further improved by increasing the Q -ratio of coil elements that were further from the sample (*i.e.*, less loaded with Q -ratios closer to 2.0).

Parallel imaging and geometric distortions

Geometry-factor maps (Fig. 7) demonstrate moderate increases in the mean noise amplification (20%, 10%, and 37%) with linear reduction factors of three-fold in the left–right, anterior–posterior, and superior–inferior directions, respectively. This is due to the three-dimensional layout of coil elements on the former. Noise amplification occurs at an increased rate as the reduction factor increases to four-fold, most notably in the superior–inferior direction where there are fewer coil elements. The coil allows for acceleration along all three Cartesian axes; this flexibility can be useful when implementing different protocols (for example, two- versus three-dimensional acquisitions), as demonstrated in this study by accelerating along different axes for the MP2RAGE and EPI acquisitions.

Static-field variations caused by magnetic-susceptibility gradients are linearly dependent on the strength of the static magnetic field. At ultrahigh field, this results in geometric distortions in sequences with long echo trains, as evidenced by the fully encoded echo-planar image of Fig. 8. Implementing a two-fold reduction factor and partial-Fourier encoding allowed for a shortened echo train, thereby substantially reducing geometric distortion in single-shot EPI. The close proximity of the receive coil to the brain, coupled with low noise amplification during image reconstruction, allowed for short echo trains while maintaining sufficient temporal SNR. Janssens et al. (2013) have compared the SNR and noise amplification of single-channel, four-channel, and

22-channel receive coils to demonstrate the increase in performance attained by increasing the number of receivers.

Conclusions

An 8-channel transmit coil and 24-channel receive coil were developed to address the challenges inherent to whole-brain monkey imaging at 7 T. It was demonstrated that there is a significant advantage to using a parallel-transmit coil for monkey imaging at ultrahigh field. The transmit coil was capable of improving both the efficiency and uniformity of the transmit field, over the traditional circularly polarized mode (representative of a single-channel volume coil), by adjusting the magnitude and phase of individual transmit channels. The transmit-field uniformity was demonstrated in a TSE image; the combination of high transmit uniformity and high transmit efficiency was demonstrated in an MP2RAGE image, wherein the adiabatic condition was met throughout the brain.

The receive coil was designed to accommodate a head-fixation post and recording chambers, while fitting close to the head. Sensitivity was achieved over the whole brain and parallel acceleration was possible along an arbitrary axis: EPI acquisitions could then be accelerated to minimize geometric distortions with low noise amplification during image reconstruction.

The transmit and receive coils provided a practical solution for producing whole-brain anatomical images and EPI time courses of monkeys at ultrahigh field. It was demonstrated that there are compelling benefits to implementing parallel-transmit coils for monkey imaging at ultrahigh-field strengths.

Acknowledgments

The authors would like to thank Nicole Hague and Ashley Kirley for animal care and preparation. This work was supported by the Canadian Institutes of Health Research (MOP-111085, MOP-89785), Canada Foundation for Innovation (30812), and Canada Research Chairs.

References

- Adriany, G., Auerbach, E.J., Snyder, C.J., Gozubuyuk, A., Moeller, S., Ritter, J., van de Moortele, P.F., Vaughan, T., Ugurbil, K., 2010a. A 32-channel lattice transmission line array for parallel transmit and receive MRI at 7 Tesla. *Magn. Reson. Med.* 63, 1478–1485.
- Adriany, G., Harel, N., Yacoub, E., Moeller, S., Ghose, G., Ugurbil, K., 2010b. A 21 channel transceiver array for non-human primate applications at 7 Tesla. *Proceedings of the 18th Annual Meeting of ISMRM*, p. 1490.
- Adriany, G., Waks, M., Tramm, B., Schillak, S., Yacoub, E., de Martino, F., van de Moortele, P.-F., Naselaris, T., Olman, C., Vaughan, T., Ugurbil, K., 2012. An open faced 4 ch. Loop transmit/16 ch. Receive array coil for hires fMRI at 7 Tesla. *Proceedings of the 20th Annual Meeting of ISMRM*, p. 429.
- Barazany, D., Assaf, Y., 2012. Visualization of cortical lamination patterns with magnetic resonance imaging. *Cereb. Cortex* 22, 2016–2023.
- Chen, G., Wang, F., Gore, J.C., Roe, A.W., 2012. Identification of cortical lamination in awake monkeys by high resolution magnetic resonance imaging. *NeuroImage* 59, 3441–3449.
- Chen, G., Wang, F., Gore, J.C., Roe, A.W., 2013. Layer-specific bold activation in awake monkey v1 revealed by ultra-high spatial resolution functional magnetic resonance imaging. *NeuroImage* 64, 147–155.
- Curtis, A.T., Gilbert, K.M., Klassen, L.M., Gati, J.S., Menon, R.S., 2012. Slice-by-slice B1 + shimming at 7 T. *Magn. Reson. Med.* 68, 1109–1116.
- Dubowitz, D.J., Chen, D.Y., Atkinson, D.J., Grieve, K.L., Gillikin, B., Bradley, W.G., Andersen, R.A., 1998. Functional magnetic resonance imaging in macaque cortex. *Neuroreport* 9, 2213–2218.
- Ekstrom, L.B., Roelfsema, P.R., Arsenault, J.T., Bonmassar, G., Vanduffel, W., 2008. Bottom-up dependent gating of frontal signals in early visual cortex. *Science* 321, 414–417.
- Gilbert, K.M., Curtis, A.T., Gati, J.S., Klassen, L.M., Menon, R.S., 2010. A radiofrequency coil to facilitate B_1^+ shimming and parallel imaging acceleration in three dimensions at 7 T. *NMR Biomed.* 24, 815–823.
- Gilbert, K.M., DiPrimio, M., Hughes, S., Manning, K.Y., Menon, R.S., 2013. Whole-brain and local receive arrays for imaging non-human primates. *Proceedings of the 21st Annual Meeting of ISMRM*, p. 3008.
- Goense, J., Logothetis, N.K., Merkle, H., 2010. Flexible, phase-matched, linear receive arrays for high-field MRI in monkeys. *Magn. Reson. Imaging* 28, 1183–1191.
- Goense, J., Merkle, H., Logothetis, N.K., 2012. High-resolution fMRI reveals laminar differences in neurovascular coupling between positive and negative bold responses. *Neuron* 76, 629–639.

- Gonen, O., Liu, S.L., Goelman, G., Ratai, E.M., Pilkenton, S., Lentz, M.R., Gonzalez, G., 2008. Proton MR spectroscopic imaging of rhesus macaque brain in vivo at 7 T. *Magn. Reson. Med.* 59, 692–699.
- Griswold, M.A., Jakob, P.M., Heidemann, R.M., Nittka, M., Jellus, V., Wang, J.M., Kiefer, B., Haase, A., 2002. Generalized autocalibrating partially parallel acquisitions (GRAPPA). *Magn. Reson. Med.* 47, 1202–1210.
- Helms, G., Garea-Rodriguez, E., Schlumbohm, C., König, J., Dechent, P., Fuchs, E., Wilke, M., 2013. Structural and quantitative neuroimaging of the common marmoset monkey using a clinical MRI system. *J. Neurosci. Methods* 215, 121–131.
- Janssens, T., Keil, B., Farivar, R., McNab, J.A., Polimeni, J.R., Gerits, A., Arsenault, J.T., Wald, L.L., Vanduffel, W., 2012. An implanted 8-channel array coil for high-resolution macaque MRI at 3 T. *NeuroImage* 62, 1529–1536.
- Janssens, T., Keil, B., Serano, P., Mareyam, A., McNab, J.A., Wald, L.L., Vanduffel, W., 2013. A 22-channel receive array with helmholtz transmit coil for anesthetized macaque MRI at 3 T. *NMR Biomed.* 26, 1431–1440.
- Khachaturian, M.H., 2010. A 4-channel 3 Tesla phased array receive coil for awake rhesus monkey fMRI and diffusion MRI experiments. *J. Biomed. Sci. Eng.* 3, 1085–1092.
- Kolster, H., Mandeville, J.B., Vanduffel, W., Wald, L.L., 2007. Methodology for sub-millimeter resolution fMRI in awake monkeys at 7 T. *Proceedings of the 15th Annual Meeting of ISMRM*, p. 119.
- Logothetis, N.K., Guggenberger, H., Peled, S., Pauls, J., 1999. Functional imaging of the monkey brain. *Nat. Neurosci.* 2, 555–562.
- Logothetis, N.K., Pauls, J., Augath, M., Trinath, T., Oeltermann, A., 2001. Neurophysiological investigation of the basis of the fMRI signal. *Nature* 412, 150–157.
- Logothetis, N.K., Merkle, H., Augath, M., Trinath, T., Ugurbil, K., 2002. Ultra high-resolution fMRI in monkeys with implanted RF coils. *Neuron* 35, 227–242.
- Mao, W.H., Smith, M.B., Collins, C.M., 2006. Exploring the limits of RF shimming for high-field MRI of the human head. *Magn. Reson. Med.* 56, 918–922.
- Mareyam, A., Blau, J., Polimeni, J., Keil, B., Farivar, R., Benner, T., Vanduffel, W., Wald, L.L., 2011. Eight-channel array coil optimized for functional imaging of awake monkeys at 7 T. *Proceedings of the 19th Annual Meeting of ISMRM*, p. 1823.
- Moeller, S., Freiwald, W.A., Tsao, D.Y., 2008. Patches with links: a unified system for processing faces in the macaque temporal lobe. *Science* 320, 1355–1359.
- Moeller, S., Yacoub, E., Olfman, C.A., Auerbach, E., Strupp, J., Harel, N., Ugurbil, K., 2010. Multiband multislice GE-EPI at 7 Tesla, with 16-fold acceleration using partial parallel imaging with application to high spatial and temporal whole-brain fMRI. *Magn. Reson. Med.* 63, 1144–1153.
- Nehrke, K., 2009. On the steady-state properties of actual flip angle imaging (AFI). *Magn. Reson. Med.* 61, 84–92.
- Papoti, D., Yen, C.C.-C., Mackel, J.B., Merkle, H., Silva, A.C., 2013. An embedded four-channel receive-only RF coil array for fMRI experiments of the somatosensory pathway in conscious awake marmosets. *NMR Biomed.* 26, 1395–1402.
- Pfeuffer, J., Merkle, H., Beyerlein, M., Steudel, T., Logothetis, N.K., 2004. Anatomical and functional MR imaging in the macaque monkey using a vertical large-bore 7 Tesla setup. *Magn. Reson. Imaging* 22, 1343–1359.
- Pfeuffer, J., Shmuel, A., Keliris, G.A., Steudel, T., Merkle, H., Logothetis, N.K., 2007. Functional MR imaging in the awake monkey: effects of motion on dynamic off-resonance and processing strategies. *Magn. Reson. Imaging* 25, 869–882.
- Pruessmann, K.P., Weiger, M., Scheidegger, M.B., Boesiger, P., 1999. SENSE: sensitivity encoding for fast MRI. *Magn. Reson. Med.* 42, 952–962.
- Reeder, S., 2007. Measurement of signal-to-noise ratio and parallel imaging. In: Schoenberg, S.O., Dietrich, O., Reiser, M. (Eds.), *Parallel Imaging in Clinical MR Applications*. Springer, Berlin, pp. 49–61.
- Roemer, P.B., Edelstein, W.A., Hayes, C.E., Souza, S.P., Mueller, O.M., 1990. The NMR phased-array. *Magn. Reson. Med.* 16, 192–225.
- Roopnarane, C.A., Ryu, Y.C., Tofighi, M.R., Miller, P.A., Oh, S., Wang, J.L., Park, B.S., Ansel, L., Lieu, C.A., Subramanian, T., Yang, Q.X., Collins, C.M., 2012. Quadrature RF coil for in vivo brain MRI of a macaque monkey in a stereotaxic head frame. *Concepts Magn. Reson Part B* 41B, 22–27.
- Sodickson, D.K., Manning, W.J., 1997. Simultaneous acquisition of spatial harmonics (SMASH): fast imaging with radiofrequency coil arrays. *Magn. Reson. Med.* 38, 591–603.
- Van de Moortele, P.F., Akgun, C., Adriany, G., Moeller, S., Ritter, J., Collins, C.M., Smith, M.B., Vaughan, J.T., Ugurbil, K., 2005. B_1 destructive interferences and spatial phase patterns at 7 T with a head transceiver array coil. *Magn. Reson. Med.* 54, 1503–1518.
- Vanduffel, W., Fize, D., Mandeville, J.B., Nelissen, K., Van Hecke, P., Rosen, B.R., Tootell, R.B.H., Orban, G.A., 2001. Visual motion processing investigated using contrast agent-enhanced fMRI in awake behaving monkeys. *Neuron* 32, 565–577.
- Wiesinger, F., Van de Moortele, P.F., Adriany, G., De Zanche, N., Ugurbil, K., Pruessmann, K.P., 2004. Parallel imaging performance as a function of field strength — an experimental investigation using electrodynamic scaling. *Magn. Reson. Med.* 52, 953–964.
- Yarnykh, V.L., 2007. Actual flip-angle imaging in the pulsed steady state: a method for rapid three-dimensional mapping of the transmitted radiofrequency field. *Magn. Reson. Med.* 57, 192–200.
- You, Z., Kwok, W.E., Mukherjee, M., Mancarella, M., 2007. 3D-orthogonal phased array coil for high-resolution and low-distortion EPI imaging of monkey brain at 3.0 T. *Proceedings of the 15th Annual Meeting of ISMRM*, p. 1040.
- Zhao, W., Cohen-Adad, J., Polimeni, J.R., Keil, B., Guerin, B., Setsompop, K., Serano, P., Mareyam, A., Hoecht, P., Wald, L.L., 2014. Nineteen-channel receive array and four-channel transmit array coil for cervical spinal cord imaging at 7 T. *Magn. Reson. Med.* 72, 291–300.
- Zitella, L.M., Xiao, Y., Teplitzky, B.A., Kastl, D.J., Duchin, Y., Baker, K.B., Vitek, J.L., Adriany, G., Yacoub, E., Harel, N., Johnson, M.D., 2015. *In vivo* 7 T MRI of the non-human primate brainstem. *PLoS ONE* 10, 1–18.